X-RAY AND RADIO VARIABILITY OF M31, THE ANDROMEDA GALAXY NUCLEAR SUPERMASSIVE BLACK HOLE*

Citation: Garcia, Michael R., Richard Hextall, Frederick K. Baganoff, Jose Galache, Fulvio Melia, Stephen S. Murray, F. A. Primini, Loránt O. Sjouwerman, and Ben Williams. "X-RAY AND RADIO VARIABILITY OF M31*, THE ANDROMEDA GALAXY NUCLEAR SUPERMASSIVE BLACK HOLE." The Astrophysical Journal 710, no. 1 (January 21, 2010): 755–763. © 2009 American Astronomical Society.

As Published: http://dx.doi.org/10.1088/0004-637x/710/1/755

Publisher: Institute of Physics/American Astronomical Society

Persistent URL: http://hdl.handle.net/1721.1/96091

Version: Final published version: final published article, as it appeared in a journal, conference proceedings, or other formally published context

The Astrophysical Journal, 710:755–763, 2010 February 10 doi:10.1088/0004-637X/710/1/755

X-RAY AND RADIO VARIABILITY OF M31*, THE ANDROMEDA GALAXY NUCLEAR SUPERMASSIVE BLACK HOLE

Michael R. Garcia[1], Richard Hextall[1,2], Frederick K. Baganoff[3], Jose Galache[1], Fulvio Melia[4], Stephen S. Murray[1], F. A. Primini[1], Loránt O. Sjouwerman[5], and Ben Williams[6]
[1] Harvard-Smithsonian Center for Astrophysics, 60 Garden Street, Cambridge, MA 02138, USA; garcia@head.cfa.harvard.edu
[2] Department of Physics, University of Southampton, UK
[3] Kavli Institute for Astrophysics and Space Research, Massachusetts Institute of Technology, Cambridge, MA 02138, USA
[4] Physics Department, The Applied Math Program, and Steward Observatory, The University of Arizona, Tucson, AZ 85721, USA
[5] National Radio Astronomy Observatory, Socorro, NM 87801, USA
[6] Department of Astronomy, University of Washington, Seattle, WA 98195, USA
Received 2009 July 28; accepted 2010 January 3; published 2010 January 21

ABSTRACT

We confirm our earlier tentative detection of M31* in X-rays and measure its light curve and spectrum. Observations in 2004–2005 find M31* rather quiescent in the X-ray and radio. However, X-ray observations in 2006–2007 show M31* to be highly variable at times. A separate variable X-ray source is found near P1, the brighter of the two optical nuclei. The apparent angular Bondi radius of M31* is the largest of any black hole and large enough to be well resolved with *Chandra*. The diffuse emission within this Bondi radius is found to have an X-ray temperature ∼0.3 keV and density 0.1 cm^{-3}, indistinguishable from the hot gas in the surrounding regions of the bulge given the statistics allowed by the current observations. The X-ray source at the location of M31* is consistent with a point source and a power-law spectrum with energy slope 0.9 ± 0.2. Our identification of this X-ray source with M31* is based solely on positional coincidence.

Key words: accretion, accretion disks – black hole physics – galaxies: individual (M31) – galaxies: nuclei

Online-only material: color figures

1. INTRODUCTION

Supermassive Black Holes (SMBHs) in galactic nuclei spend the vast majority of their life accreting at very low rates, but our understanding of how this accretion occurs is relatively poor compared to our understanding of what happens at high rates. At high rates, a slim accretion disk often forms and ∼10% of the accretion energy is radiated. At low rates, the accretion becomes radiatively inefficient, but we are uncertain what fraction of the accretion energy is radiated, and what fraction of the gas accreted at large radii actually reaches the black hole event horizon. A straightforward way to determine how much mass is accreted is to image the accretion flow and therefore determine the run of density with radius.

Perhaps the best candidate for such a study is the SMBH in M31. Following the nomenclature used in the Galaxy, where Sgr A* is used to refer to the central SMBH, we hereafter refer to the central SMBH in M31 as M31*. The mass of M31* has previously been estimated as $3 \times 10^7\ M_\odot$ (Kormendy & Bender 1999), but more recent *Hubble Space Telescope* (*HST*) spectroscopy indicates that the mass is $1.4^{+0.7}_{-0.3} \times 10^8\ M_\odot$ (Bender et al. 2005). This higher mass means the Bondi radius is not the 0.″9 previously estimated (Garcia et al. 2005, 3.4 pc at the 780 kpc distance to M31; Stanek & Garnavich 1998) but ∼5″ (=18 pc, see below), making it the largest of any known SMBH. Given the resolution of *Chandra* of ∼0.″6, there are only three SMBH with Bondi radii which can be resolved in the X-ray (M87, Sgr A*, and M31*). Among these three, the Bondi radius of M31* is the most highly resolved, so detection of the accretion flow within it would have the most power to determine the run of density with radius.

Within the Bondi radius, *Chandra* detects several point sources and also diffuse gas which is present throughout the bulge of M31 (Shirey et al. 2001a; Takahashi et al. 2004; Li & Wang 2007a). Our earlier work (Garcia et al. 2000) suggested that a super-soft point source near the nucleus was the X-ray counterpart of M31*, but subsequent alignment with M31 globular clusters (Barmby & Huchra 2001) revealed that this was not the case (Garcia et al. 2001, 2005). *Chandra* HRC imaging revealed that the X-ray source closest to the nucleus is made up of two partially resolved components, one of which is within ∼0.″1 of the position of the SMBH and which we tentatively identified as the $\sim 10^{36}$ erg s^{-1} X-ray counterpart of M31* (Garcia et al. 2005). This earlier work was based on only 13 photons and "While very suggestive ... clearly needs confirmation" (quoting from that work). In this work, we confirm the detection and measure the variability of this SMBH.

Hubble imaging revealed an unusual double nucleus within M31 (Lauer et al. 1993) which has been successfully modeled as an eccentric torus of stars viewed nearly edge on (Tremaine 1995). The optically brighter end of the torus is known as P1, the optically fainter (but UV brighter) end as P2. More recent Hubble imaging and spectroscopy revealed that embedded within P2 is a dense cluster of several hundred A-stars which are very UV bright. This cluster has been dubbed P3 and its brightness peaks at essentially the same position as that of P2 (Bender et al. 2005). *HST* spectroscopy reveals a dark mass (presumed black hole) located at the center of this cluster with an estimated mass of $1.4^{+0.7}_{-0.3} \times 10^8\ M_\odot$ (Bender et al. 2005). The presence of so many young A stars in the nucleus of M31, which otherwise is made up of an old stellar population, is a mystery. The same phenomenon is also seen near Sgr A* (Ghez et al. 2003a). Demarque & Virani (2007) suggest that these apparently young stars may actually be old and relics of stellar collisions in the very dense nuclear regions, but recent *HST* spectra indicate that at least in the case of the Galactic center these are genuine young, massive stars (Ghez et al. 2003b; Martins et al. 2008). A suggested source for the gas which later collapses to form

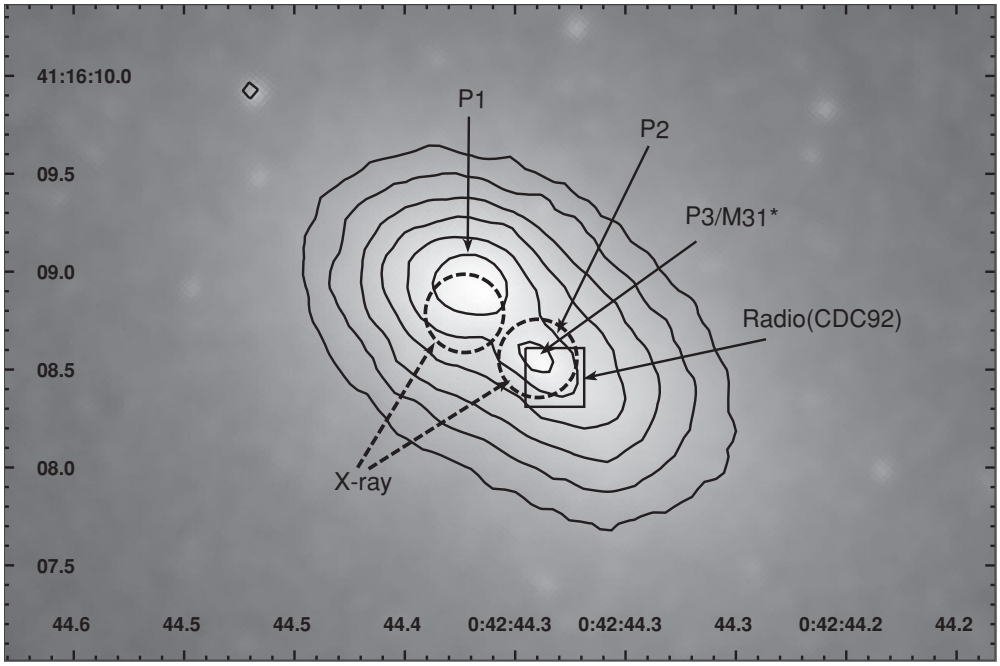

Figure 1. Diagram showing the relative locations of objects at different wavebands within the M31 triple nucleus. The background is the *HST* F435W image, registered to the LGS (Massey et al. 2006). Co-ordinates are J2000 and have an absolute accuracy of ∼0.″3. The contours are derived from the F435W image. At optical and near-IR wavelengths, the brightest peak in the nucleus is P1 (upper left of center). The next brightest is P2 (to the southwest). At UV wavelengths, the brightest object is P3, a tiny cluster at the same location as P2. The SMBH M31* is within 0.″02 of the center of P3. See Bender et al. (2005), in particular Figure 2, panel 2, for a more detailed description. The location of the unresolved radio source discovered by Crane et al. (1993) is shown by a square 0.″3 on a side, corresponding to the positional error of the radio source. The location of the two nuclear X-ray sources discussed herein is shown as dashed circles 0.″2 in radius, corresponding to the accuracy of the *HST*/*Chandra* registration. Readers may find helpful the similar diagram in Melia (1992b), but should note that this work predates the discovery of the triple nucleus.

the P3 star cluster is stellar mass loss from the older stars in the orbiting torus (Chang et al. 2007).

Spitzer imaging reveals that M31 looks less like a spiral galaxy than previously thought. Instead, the warm gas and dust is in the form of a set of rings, apparently due to transits of M32 through the center of the plane of the M31 disk (Barmby et al. 2006; Gordon et al. 2006). The most recent of these transits took place 210 million years ago (Block et al. 2006) and would have triggered a burst of star formation.

The association of the radio source (∼30 μJy at 3.6 cm) with a nuclear black hole by Crane et al. (1993) and Melia (1992b) and subsequently by all others so far is supported by the detection of an unresolved (<1 pc or 0.″35) radio source at the position of the stellar nucleus (within ∼ 1/2″; Garcia et al. 2005), and radio variability which is comparable to the radio variability of Sgr A* (Sjouwerman et al. 2005). Figure 1 shows the locations of the multi-wavelength components of the M31 nucleus. While there is little doubt the source of this radio emission is M31*, direct registration of the radio and X-ray and/or radio and *HST* images, perhaps using background QSOs, could reduce this positional uncertainty. We limit ourselves here to direct registration of the X-ray and *HST* images. Table 1 shows the absolute (J2000) co-ordinates of the X-ray, optical, and radio objects of interest in the nucleus. The errors associated with these measurements are described below.

While M31* is 100× further away than the SMBH in the center of our Galaxy, it suffers much less reddening: $A_V \sim 1$ (Garcia et al. 2000), whereas $A_V \sim 30$ for Sgr A*. The dominant temperature of the diffuse gas in the core of M31 is ∼0.3 keV (Dosaj et al. 2001; Shirey et al. 2001b; Li & Wang 2007b; Bogdan & Gilfanov 2008) as compared to 1.0 keV (Baganoff et al. 2003) around Sgr A*. A comparative study of these two closest SMBH (M31* and Sgr A*) will deepen our understanding of the physics of black hole accretion and emission mechanisms at low rates. In this regard, M31* and Sgr A* offer interesting differences in that M31* is 3× less luminous in the radio but 1–3 orders of magnitude more luminous in the X-ray.

Table 1
Co-ordinates of X-ray, Optical, and Radio Nuclear Sources

Object	R.A. (J2000)	Decl. (J2000)	Error[a]
P1 *HST*	00:42:44.37	41:16:08.9	0.″3
P2 *HST*	00:42:44.34	41:16:08.5	0.″3
P3 *HST*	00:42:44.34	41:16:08.5	0.″3
M31*	00:42:44.34	41:16:08.5	0.″3
Radio	00:42:44.33	41:16:08.4	0.″15 [b]
P1 X-ray	00:42:44.37	41:16:08.8	0.″36 [c]
P3 X-ray	00:42:44.34	41:16:08.6	0.″36 [c]

Notes.
[a] The error in the absolute coordinates is set by the coordinate system of the LGS data, which is accurate to ∼0.″3 (Massey et al. 2006).
[b] Position from Crane et al. (1993) corrected for the type-o in Table 1 therein.
[c] Absolute errors in the X-ray positions include the quadrature sum of the LGS (0.″3) plus registration (0.″2) errors, 0.″36.

2. OBSERVATIONS

M31 has been observed extensively with both *Chandra* (i.e., Garcia et al. 2000; Kong et al. 2003; Williams et al. 2006; Di Stefano et al. 2004) and *XMM-Newton* (i.e., Shirey et al. 2001b; Pietsch et al. 2007). Many of the *Chandra* observations have been in the form of monthly short (∼5 ks) snapshots in order to monitor the variability of the point source population, but there also have been longer observations to search for rapid variability (Kaaret 2002) and to study source populations

Table 2
Observation IDs, Dates, Exposure Times, and Nominal Aim Points for the 16 *Chandra* HRC Images Discussed in this Paper

Obs-id	Start Date	Exposure Time (ks)	Aim Point (J2000) R.A.	Decl.
1912	2001 Nov 1	50.0	00 42 42.30	+41 16 08.40
5925	2004 Dec 6	46.7	00 42 44.40	+41 16 08.30
6177	2004 Dec 27	20.2	00 42 44.40	+41 16 08.30
5926	2004 Dec 27	28.5	00 42 44.40	+41 16 08.30
6202	2005 Jan 28	18.2	00 42 44.40	+41 16 08.30
5927	2005 Jan 28	27.2	00 42 44.40	+41 16 08.30
5928	2005 Feb 21	45.2	00 42 44.40	+41 16 08.30
7283	2006 Jun 5	20.1	00 42 44.30	+41 16 09.40
7284	2006 Sep 30	20.2	00 42 44.30	+41 16 09.40
7285	2006 Nov 13	18.7	00 42 44.30	+41 16 09.40
7286	2007 Mar 11	19.1	00 42 44.30	+41 16 09.40
8526	2007 Nov 7	20.2	00 42 44.30	+41 16 09.40
8527	2007 Nov 17	20.2	00 42 44.30	+41 16 09.40
8528	2007 Nov 28	20.2	00 42 44.30	+41 16 09.40
8529	2007 Dec 7	19.1	00 42 44.30	+41 16 09.40
8530	2007 Dec 17	20.1	00 42 44.30	+41 16 09.40

(Di Stefano et al. 2004; Pietsch et al. 2007). The total *Chandra* exposure on M31 is now ∼1.3 Ms and it continues to climb. If one limits the selection of data to only those taken with ACIS-I within 1 arcmin of the nucleus, the total exposure is currently ∼250 ks. While *Chandra* is able to view M31 10 months out of every year, visibility from *XMM-Newton* is restricted to a few week long window every 6 months, so the *XMM-Newton* observations have taken the form of less frequent, but longer, exposures (Trudolyubov et al. 2005).

The *Chandra* observations discovered the first resolved SNR in an external galaxy (Kong et al. 2002a), and summed *Chandra* observations have provided a fiducial point for X-ray color–color diagrams which help to separate unresolved X-ray source populations in more distant galaxies into SNR, high and low mass X-ray binaries, and background active galactic nucleus (AGN; Kong et al. 2002b; Prestwich et al. 2003). These datasets have also revealed extensive structure in the diffuse emission (Li & Wang 2007b; Bogdan & Gilfanov 2008). Multi-wavelength studies of the M31* environment suggest the presence of an outflow of hot gas from the nuclear region (Li et al. 2009).

Below we discuss the datasets analyzed in this paper; first, those taken with the *Chandra* HRC and then those taken with the *Chandra* ACIS.

2.1. Chandra HRC Observations

In 2004/2005, we undertook a series of four moderate (50 ks) HRC-I exposures separated by 1 month in order to confirm our earlier possible detection of M31* and to search for any variability. Two of these exposures were subdivided into approximately equal sections and separated by the normal 10 hr pause in observations, while *Chandra* transits the Earth's radiation belts. We also include in our analysis archival HRC observations made during 2006/2007 which were designed to monitor optical nova (Henze et al. 2009), and a single 50 ks observation from 2001 (Kaaret 2002). Table 2 lists the dataset we have analyzed, giving observation dates and exposure times.

In order to identify M31* within the *Chandra* images and then extract a light curve, it was first necessary to accurately determine the location of M31* within the HRC images. The absolute astrometric accuracy of *HST* and *Chandra* images is

Table 3
Observation IDs, Dates, Start Times, and Exposure Times for the 29 ACIS-I Images Merged Together and Shown in Figure 6 (Left)

Obs-id	Start Date	Exposure Time (ks)	Aim Point (J2000) R.A.	Decl.
303	1999 Oct 13	11.8	00 42 44.40	+41 16 08.30
305	1999 Dec 11	4.1	00 42 44.40	+41 16 08.30
306	1999 Dec 27	4.1	00 42 44.40	+41 16 08.30
307	2000 Jan 1	4.1	00 42 44.40	+41 16 08.30
308	2000 Feb 16	4.0	00 42 44.40	+41 16 08.30
311	2000 Jul 29	4.9	00 42 44.40	+41 16 08.30
312	2000 Aug 27	4.7	00 42 44.40	+41 16 08.30
1581	2000 Dec 13	4.4	00 42 44.40	+41 16 08.30
1582	2001 Feb 18	4.3	00 42 44.40	+41 16 08.30
1583	2001 Jun 10	4.9	00 42 44.40	+41 16 08.30
4360	2002 Aug 11	4.9	00 42 44.40	+41 16 08.90
4678	2003 Nov 9	3.9	00 42 44.40	+41 16 08.30
4679	2003 Nov 26	3.8	00 42 44.40	+41 16 08.30
4680	2003 Dec 27	4.2	00 42 44.40	+41 16 08.30
4681	2004 Jan 31	4.2	00 42 44.40	+41 16 08.30
4682	2004 May 23	3.9	00 42 44.40	+41 16 08.30
4719	2004 Jul 17	4.1	00 42 44.30	+41 16 08.40
4720	2004 Sep 2	4.1	00 42 44.30	+41 16 08.40
4721	2004 Oct 4	4.1	00 42 44.30	+41 16 08.40
4722	2004 Oct 31	3.8	00 42 44.30	+41 16 08.40
7064	2006 Dec 4	23.2	00 42 44.40	+41 16 08.30
7136	2006 Jan 6	4.0	00 42 44.40	+41 16 08.30
7137	2006 May 26	3.9	00 42 44.40	+41 16 08.30
7138	2006 Jun 9	4.1	00 42 44.40	+41 16 08.30
7139	2006 Jul 31	4.0	00 42 44.40	+41 16 08.30
7140	2006 Sep 24	4.1	00 42 44.40	+41 16 08.30
8183	2007 Jan 14	4.0	00 42 44.40	+41 16 08.30
8184	2007 Feb 14	4.1	00 42 44.40	+41 16 08.30
8185	2007 Mar 10	4.0	00 42 44.40	+41 16 08.30

Note. Total exposure time is 148 ks.

$\lesssim 1''$, which is insufficient to uniquely identify sources in the crowded core of M31. Within narrow fields ($\lesssim 1'$) it is possible to register *HST* and *Chandra* images to ∼0.″1 accuracy (Edmonds et al. 2003). Over larger fields, the point-spread function (PSF) of the *Chandra* mirror increases substantially, and this along with the calibration of the HRC may limit the astrometric accuracy even with registration (Beckerman et al. 2004).

There are very few sources in common between our *Chandra* images and the *HST*/Advanced Camera for Surveys (ACS; F435W) images which show the M31 double nucleus, so we used a two-step process to register our images. As part of our search for counterparts to black hole X-ray transients (Williams et al. 2005), we obtained several *HST*/ACS images of the M31 nucleus, and one of these was first registered to the Local Group Survey (LGS; Massey et al. 2006) image of M31. The second step is to register the *Chandra* images to the same LGS image. We allow for an x and y translation, a single change in scale factor, and roll, but typically the latter two of these are negligible while the translation is significant and $<1''$.

The *HST*/ACS to LGS registration typically uses 20 stars and has a rms of 0.″03, and the registration of individual *Chandra*/HRC images to the LGS uses six or seven globular clusters and has a rms of 0.″1–0.″2. One of these seven globular clusters sometimes falls below the *Chandra* detection threshold, limiting us to six occasionally. We note that there are nine globular clusters which are in both the *Chandra* and LGS images, but two of these are between 6′ and 10′ from the nucleus where the PSF

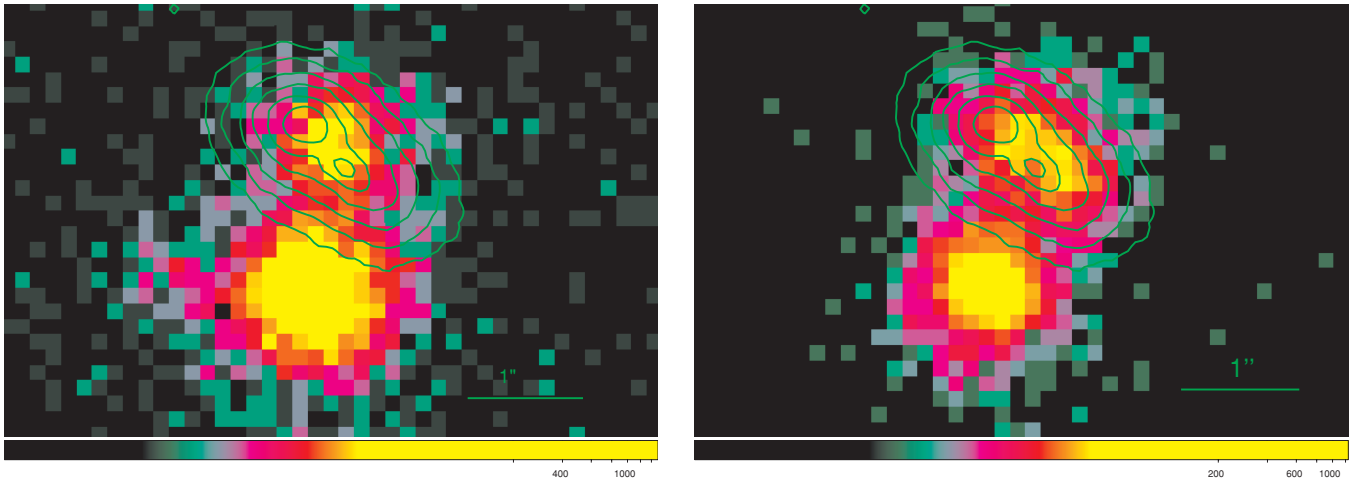

Figure 2. Summed 2001/2004/2005 (left) and 2006/2007 (right) HRC images of the M31 nucleus, registered to a common astrometric frame. The registration is accurate to ∼0.″2. The contours are from an *HST*/ACS image. The innermost contour levels are closed at the positions of P1 (upper left or northeast) and P3 (lower right) and are separated by 0.″5. In the 2004/2005 image, the source associated with P3 (=M31*) is faint, while in the 2006/2007 image, this source is stronger and clearly separate from the source near P1. The super-soft source CXO J004244.2+411608 (Garcia et al. 2000) is the bright source directly south of P1/P3.

(A color version of this figure is available in the online journal.)

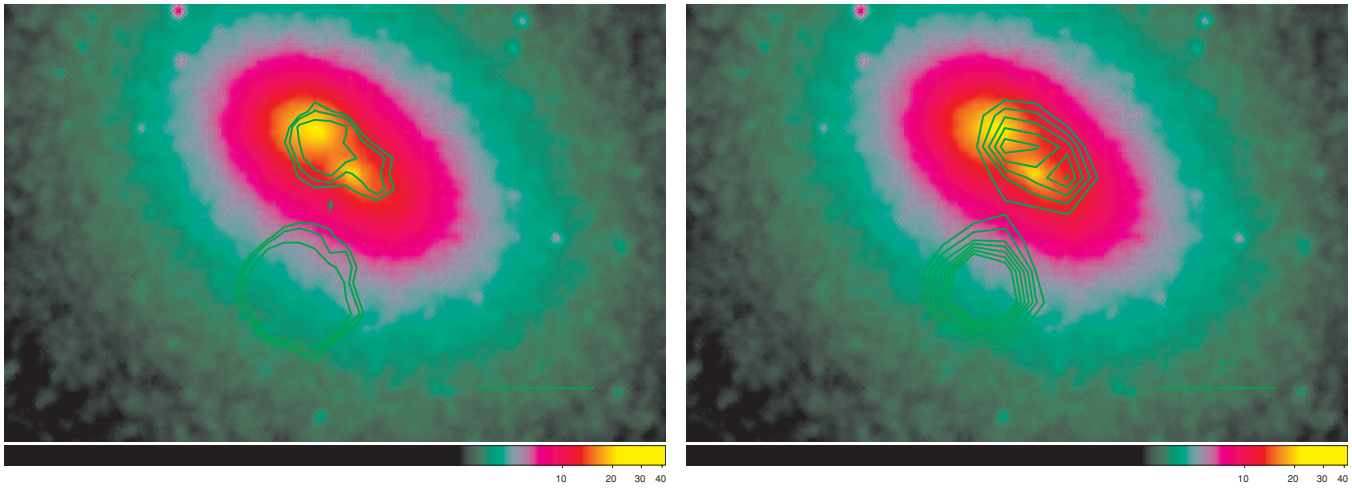

Figure 3. False color representation of the *HST*/ACS F435W image of the M31 nucleus, with the contours from the HRC images overlaid. The left image shows the contours from the summed 430 ks HRC data. The right image shows the contours from the 2006/2007 HRC data alone. A small east–west translation will bring the X-ray peaks on top of P3 and within 0.″1 of P1.

(A color version of this figure is available in the online journal.)

due to the *Chandra* mirror has widened substantially. Including these distant clusters increases the error in the registration to ∼0.″3, so we have excluded them. The remaining clusters are between 1′ and 5′ from the nucleus. Clearly the *Chandra* to LGS registration error dominates the final registration, and this error itself is dominated by the counting statistics within the PSF (and associated registration errors) in the individual globular clusters within the *Chandra* images.

In order to ensure the most accurate, and perhaps more importantly, stable, registration, we summed the HRC data into a single image and registered that image to the LGS images. The summing process (CIAO *reproject_aspect*) uses the positions of bright X-ray sources to register the individual HRC images to a common frame to better than 0.″05. The accuracy of the registration of the summed *Chandra* image to the LGS image as determined with IRAF *ccmap* is 0.″1 rms. We also summed the 2001/2004/2005 and 2006/2007 HRC data separately and registered these two images to the LGS, again finding an rms accuracy of 0.″1. Comparing these two (now registered) HRC images to each other, we find an offset between bright sources of 0.″2, larger than the formal error in the rms. Given that we are solving for four parameters (x and y shifts, scale factor, and roll) with seven points, the resulting formal rms might not be expected to be Gaussian—we therefore take 0.″2 as our de-facto registration error between the *HST* and *Chandra* images.

These two images are shown in Figure 2. The 2006/2007 image shows two separate X-ray sources at the approximate locations of P1 and P3. A simple translation of 0.″25 brings the southwestern source to the position of P3, and the northeastern source 0.″1 to the South of P1. Given the concurrence between the separation of the X-ray sources, the angle between them, and P1 and P3 as seen in the *HST* images, we identify the X-ray sources with M31* (=P3) and a source within P1. This concurrence can also be seen in Figure 3, which shows the *HST*/ACS image with the HRC contours overlaid. However, we cannot entirely exclude the possibility that one or more transient sources unrelated to P1 or P3 are responsible for the X-ray emission.

Since counting statistics of the globular clusters in the individual ∼20 ks X-ray images limit the accuracy of the

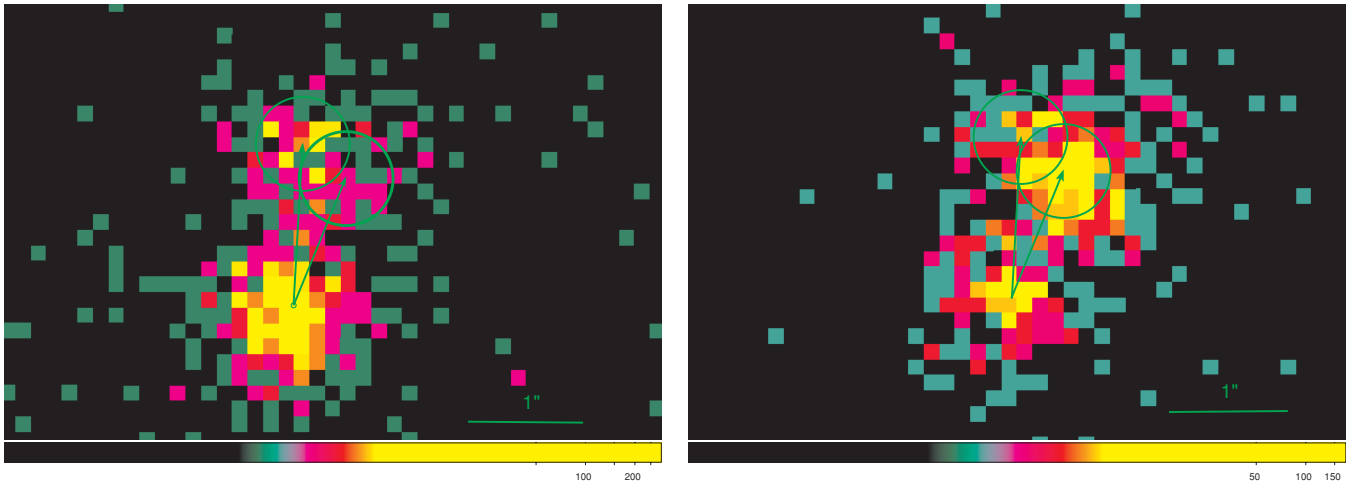

Figure 4. Two of the 15 HRC images used in our light curves. The left image from 2004 December 6.75 shows the source at P1 somewhat brighter than that at P3, while the right image from 2008 December 7 shows P3 at its brightest. The 0.″4 circles used to measure the counts are re-centered for each observation by using an identical set of vectors positioned to originate at the centroid of the super-soft source CXO J004244.2+411608 (Garcia et al. 2000) seen at the bottom of the images. Light curves were generated from the counts in these 0.″4 circles, excluding counts from the overlapping region.

(A color version of this figure is available in the online journal.)

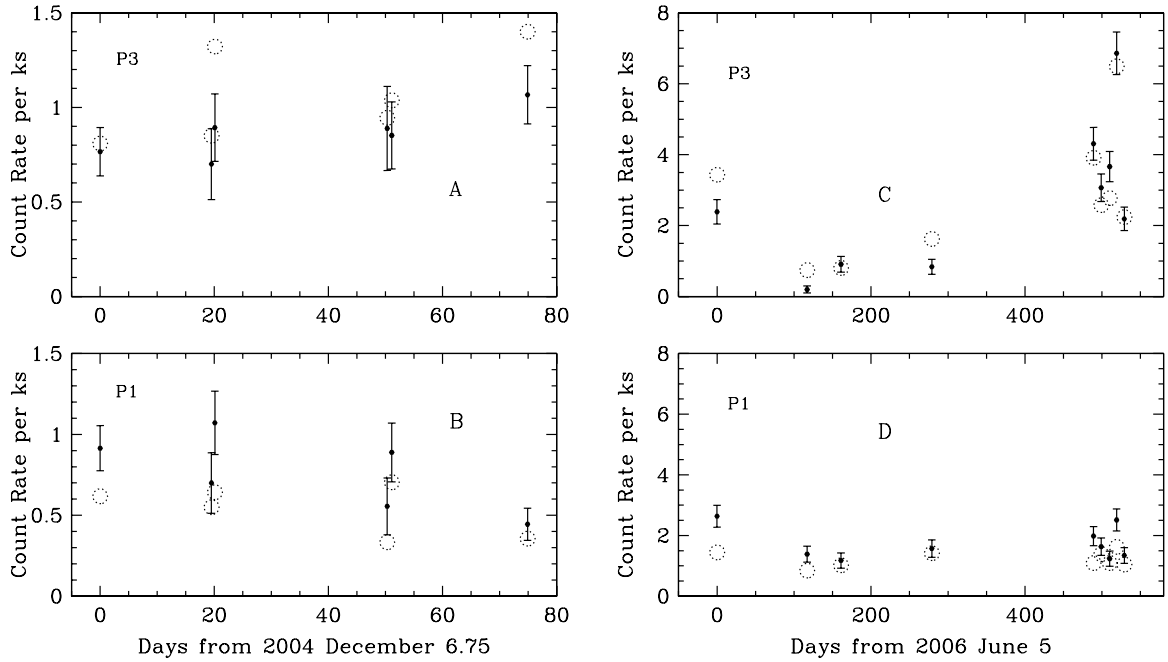

Figure 5. Light curves for P3 = M31* and the source near P1 as extracted from the HRC data. Panel A is P3 in 2004/2005, panel B P1 in 2004/2005, panel C is P3 in 2006/2007, and panel D is P1 in 2006/2007. A counting rate of 1.0 c ks^{-1} corresponds to a luminosity of 3 × 10^{36} erg s^{-1} (0.1–7.0 keV) at the 780 kpc distance of M31. Errorbars are 1σ counting statistics only. The open/dashed circles the sensitivity of the light curve to 1σ shifts in the registration and therefore count extraction procedure. We do not include the 2001 observation in the light curve due to its three-year offset.

registration, we rely on the registration of the merged 430 ks image and measure offsets to P1 and P3 from the nearby super-soft source (CXO J004244.2+411608, Garcia et al. 2000; hereafter SSS). The SSS has between 100 and 300 counts in each of the images, so can be centroided to ∼PSF/$\sqrt{}$(counts) ∼ 0.″05 in each of the individual images.

In order to extract the HRC light curves we centered extraction circles at the locations of P1 and P3 as determined by the offsets from the SSS (after the translation of 0.″25 discussed above) on each of the images and counted the photons therein. We used radii of 0.″4 centered at P1 and P3, as shown in Figure 4. P1 and P3 are sufficiently close that these circles overlap, so we excluded the counts in the overlapping region.

Figure 5 shows the resulting light curves. There is clearly some correlation between the P1 and P3 light curves, as is expected due to the proximity of the two sources. The 0.″4 extraction circle contains 50% of the flux from a point source and the two sources are only 0.″5 apart.

The most dramatic variability we find is in 2007 December (days 519–529), where M31* varies by a factor of 3 in 10 days. The maximum variability is between days 117 and 519, where we see a factor of more than 10 variation. In order to search for variability on short timescales, we divided the day 519 observation (where M31* was brightest) into five approximately equal 4000 s intervals. The rate varies by nearly a factor of 2 on between the first, second, and third intervals

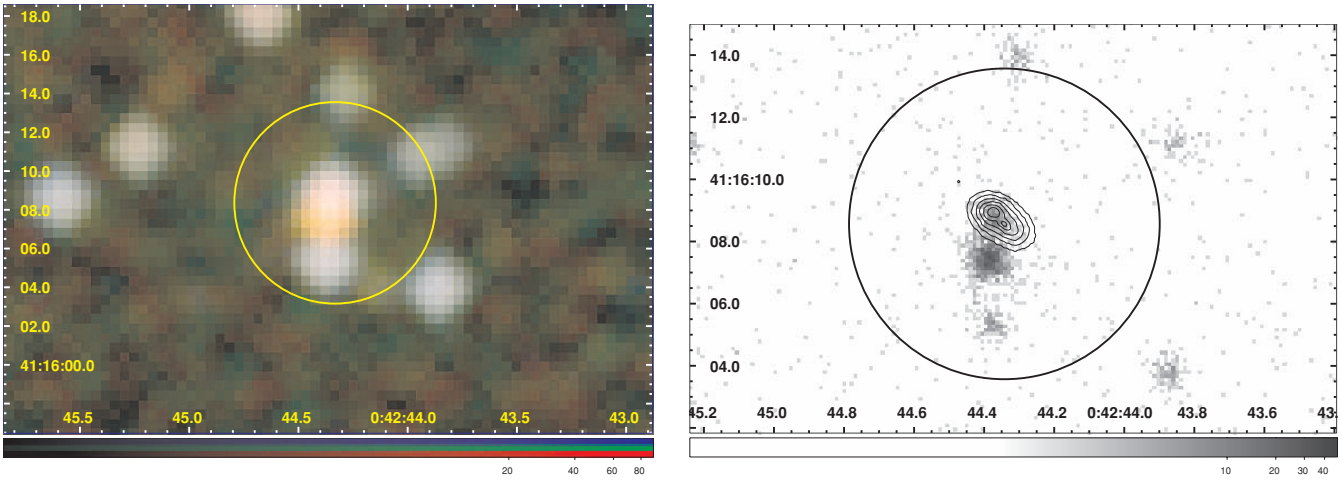

Figure 6. Left: the smoothed, summed, 148 ks exposure ACIS-I image centered on M31*. The circle is the 5.″2 = 18.7 pc Bondi radius. The color coding shows the soft band in red (0.3–1.0 keV), the medium band in green (1.0–2.5 keV) and the hard band in blue (2.5–7.0 keV). There is no clear change in the temperature of the diffuse gas at or inside of the Bondi radius. The low temperature of the super-soft source immediately to the south of M31* is apparent by its yellowish color. The flux scale is logarithmic and runs from 0 (black) to 80 counts. Right: the longest single ACIS-S exposure of M31* is this 40 ks exposure (obsid 1575). The *HST*/ACS F435W contours are overlaid and the 5.″2 Bondi radius is shown. Pixel size has been set to 0.″125 to match the HRC images shown earlier. The energy band was limited to 0.3–1.5 keV and the flux scale is logarithmic and runs from zero (white) to 40 counts in the darkest pixels.

(A color version of this figure is available in the online journal.)

(7.8 ± 1.3 counts ks^{-1}, 4.3 ± 1.1 counts ks^{-1}, 7.7 ± 1.3 counts ks^{-1}), but these variations have only ∼2σ significance and χ^2 test to the hypothesis of a constant source has a 6% chance of being satisfied, so significant variability on short timescales cannot be convincingly argued.

In order to test the sensitivity of the light curve to possible errors in the registration, we shifted the extraction circles 0.″05 both R.A. and decl., as this is the typical error in measuring the centroid of the SSS which is used as the reference point. While the overall character of the resulting light curve remains the same, some of the points do see >2σ changes (see Figure 5).

Assuming the spectral shape found with ACIS (see below) a measured rate of 1.0 counts ks^{-1} corresponds to an emitted luminosity over 0.3–7.0 keV of 2.25 × 10^{36} erg s^{-1} in the full HRC beam, or 3.0 × 10^{36} erg s^{-1} over 0.1–7.0 keV. M31* therefore ranges in luminosity from 0.6 to 20 × 10^{36} erg s^{-1} (0.1–7.0 keV). We note that if the source we associate with M31* is in fact unrelated, then these numbers are upper limits and the X-ray luminosity of M31* must at times be below 6 × 10^{35} erg s^{-1}.

2.2. *Chandra ACIS*

While the HRC data give excellent spatial resolution and allow us to determine an accurate light curve for M31*, they do not provide sufficient energy resolution to allow us to search for spectral signatures of the Bondi flow/ADAF. We therefore investigate the archival ACIS-I and ACIS-S data.

We used 29 ACIS-I exposures aimed within 1′ of M31* which total to 148 ks of exposure time. The data used is detailed in Table 3, and the summed exposure is shown in Figure 6 (left) as a smoothed three-color X-ray image where the soft (0.3–1.0 keV), medium (1.0–2.5 keV), and hard (2.5–7.0 keV) bands are color coded as red, green, and blue, respectively. The 5″ Bondi radius is shown here in yellow. The emission due to hot diffuse gas is seen throughout this image and generates ∼1 event per pixel in this image. Note that we do not include the ACIS-S observation discussed below, obsid 1575, in this sum due to the substantially different energy response of ACIS-S versus ACIS-I.

We searched for an enhancement in the flux at (or inside) of the Bondi radius by generating radial profiles of the flux, centered on M31* in several wedges that are free of point sources. Defining the ray to the north as zero degrees and moving counterclockwise, we generated these profiles over the azimuth ranges of 40°–70°, 100°–150°, and 245°–280°. In the first two of these azimuth ranges, we found a slight excess of counts near the Bondi radius (above the local background), amounting to 10 counts from 3″ to 5″ in the first region and 20 counts from 4″ to 6″ in the second region. We then used MARX to estimate the number of counts that would be scattered into these regions from the surrounding point sources, and found that this could account for ∼1/3 of the observed excess. Note that there is clear spatial structure in the diffuse emission at larger radii (10″–20″; see Li et al. 2009) which, if present at or within the Bondi radius, could easily account for the apparent excess of 10–20 counts seen in two of our regions. Assuming that the results in these three azimuth ranges are typical of what would be found for the diffuse emission at all azimuth ranges, and given that these three ranges sum to ∼1/3 of the total, we take the apparent excess of 30 total counts to correspond to a limit 3 times higher, or ∼100 counts, on any truly diffuse emission due to the Bondi flow. This limit corresponds to an emitted flux of less than 9 × 10^{-15} erg cm^{-2} s^{-1} (0.3–7.0 keV) assuming a temperature of 0.3 keV, or a luminosity at 780 kpc of <6 × 10^{35} erg s^{-1}.

Given that we do not detect a significant enhancement in the flux at (or inside) the Bondi radius, we would not expect to detect a temperature change either as any such change would need to be co-incidentally offset by a change in electron density. None the less, we did select energy bands of Figure 6 such that approximately equal counts are produced in the soft and medium bands in order that any change in the ∼0.3 keV temperature of the diffuse gas would be emphasized. As evidenced by the lack of a color change in Figure 6, there is no apparent change in the temperature of the diffuse gas at the Bondi radius.

Because spectral fitting summed ACIS data spanning many years consisting of 29 separate observations is not straightforward, we carried out a spectral analysis with the longest single

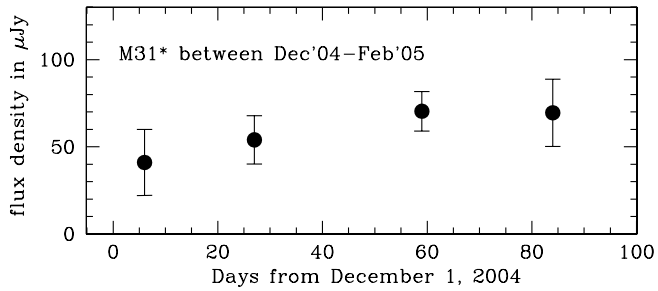

Figure 7. Day-long VLA averages at 5 GHz from our simultaneous radio/X-ray observations during 2004/2005.

ACIS observation of M31*, OBSID 1575. This 40 ks ACIS-S exposure is shown in Figure 6 (right), with Bondi radius and also the *HST* contours overlaid. Extracting the counts in a 0.″4 radius centered at M31* and excluding the overlapping region centered at P1 we find 70 counts and find a good fit to a power-law spectrum of the form $F_{\nu,x} \propto \nu^{-\alpha_{\nu,x}}$ with energy index $\alpha_{\nu,x} = 0.9 \pm 0.4$ and $N_{\rm H}$ consistent with Galactic value of 6×10^{20} cm^{-2}. Freezing $N_{\rm H}$ to be equal to the Galactic value we are able to place a tighter constraint on $\alpha_{\nu,x} = 0.9 \pm 0.2$.

Extracting the diffuse counts within the Bondi radius, and excluding the point sources, we find 182 counts. Fits to a single component model do not yield acceptable χ^2, but fits to a power-law (which is suitable to represent the undetected point sources and the small amount of scattering from the detected point sources) and a thermal spectrum are acceptable. Freezing the power law to $\alpha_{\nu,x} = 0.7$ and $N_{\rm H}$ to 6×10^{20} cm^{-2} (consistent with the Galactic value) yields a good fit ($\chi^2 = 1.3$ with 9 dof) with $kT = 0.34 \pm 0.05$. The density within this region, assuming a 5″ = 18 pc radius sphere, is measured to be ∼0.1 cm^{-3}.

2.3. VLA

We observed M31* simultaneously with the Very Large Array (VLA) at 5 GHz during our 2004/2005 *Chandra*/HRC observations. Figure 7 shows the day-long averages of the radio flux observed during these observations. We did not see any significant variability within the day long averages, to a limit of 15% on timescales of 2, 4, and 6 hr.

M31* has been observed at several radio wavelengths from the VLA, but not at the same time. Because the source is variable determining a spectrum from these observations is uncertain, but it is all the current data will allow. The mean flux densities observed at the VLA are ∼30 μJy at 8.4 GHz (measured on 1990 July, 1992 November, 1994 July, 1995 July, 1996 January), ∼50 μJy at 4.9 GHz (measured on 2002 July and August, 2003 June, July, and August, and during our monitoring simultaneous with *Chandra* in 2004 December, 2005 January and February) and between 100 and 140 μJy at 1.4 GHz (measured on 1981 August, 1986 August and September). The beam size varies from 0.″24 to 0.″4 to 1.″4, respectively at these frequencies, so one must also beware that if there is any diffuse emission it would elevate the fluxes at the lower frequencies, however the available images do not show any such emission. Taken at face value these flux densities indicate a slope $\alpha_{\nu,r} = 0.8$, where $F_{\nu,r} \propto \nu^{-\alpha_{\nu,r}}$.

3. DISCUSSION

3.1. Bondi Radius and Accretion Rate

While numerous observations make it clear that some sort of a radiatively inefficient accretion flow (RIAF) occurs onto black holes accreting at low rates, its detailed form is unclear. The accretion could proceed via a magnetically dominated inflow (Shvartsman 1971; Melia 1992a), an Advection Dominated Accretion Flow (ADAF; Narayan & Yi 1994), Convective Dominated Accretion Flow (CDAF) in which advection occurs but is moderated by convection (Igumenshchev et al. 2000; Narayan et al. 2000; Quataert & Gruzinov 2000), an ADAF and wind (in which a large fraction of the accreted material is blown out in a wind before reaching the SMBH; Narayan & Yi 1995); sometimes called an Advective Dominated Inflow Outflow Solution (ADIOS; Blandford & Begelman 1999; Hawley & Balbus 2002), or something else. One of the most promising ways to determine which of these alternatives is correct is to image the accretion flow on a sub-Bondi scale and therefore determine the structure of the flow. For example, standard ADAF flows begin at the Bondi radius and the density within the flow varies with radius R as $\rho(R) \propto R^{-3/2}$, while in the CDAF or ADAF and wind models $\rho(R) \propto R^{-3/2+P}$. Here P measures the strength of the wind/convection, with $P = 0$ corresponding to no wind and $P = 1$ to a maximal wind. Bremsstrahlung is likely to the dominant emission mechanism (Ball et al. 2001), and its emissivity $\propto \rho^2$ will enhance the observable difference in the structure of the flow.

We have previously estimated the Bondi radius and accretion rate of M31* (Garcia et al. 2005). Herein we update that estimation using the same methods. The Bondi radius is $R_B = 2GM_{BH}/c_s^2$, where the sound speed $c_s = (\gamma kT/\mu M_H)^{1/2}$. Here the adiabatic index $\gamma = 5/3$ and the mean atomic weight of the gas $\mu = 0.7$ (which implies twice the solar abundance). The Bondi accretion rate is $\dot{M}_B = \pi (GM_{BH})^2 \rho c_s^{-3}$ where $\rho = n_e \mu m_H$. We measure the temperature of the diffuse gas within 5″ = 18 pc of M31* to be 0.34 ± 0.05 keV, consistent with what has been previously measured in the inner ∼1′ (Takahashi et al. 2004; Li & Wang 2007a; Bogdan & Gilfanov 2008). This temperature and the new mass estimate lead to a Bondi radius of 5.″2 = 18.7 pc at 780 kpc. The density in the inner 1″ = 3.6 pc has been estimated at 0.06 cm^{-3} (Li & Wang 2007a) and 0.1 cm^{-3} (Takahashi et al. 2004; Dosaj et al. 2001). Herein we find a density of 0.1 cm^{-3} within the Bondi radius, leading to a Bondi accretion rate of $7 \times 10^{-5}\ M_\odot$ yr^{-1} and a Bondi luminosity of 4×10^{41} erg s^{-1}. Given the observed luminosity of $\sim 2 \times 10^{36}$ erg s^{-1} this leads to an under-luminosity of 5×10^{-6} as shown in Figure 8.

While the Bondi rate is the standard with which to compare SMBHs and to search for evidence of RIAFs, it assumes that the gas is stationary at the Bondi radius. Winds from stars, supernovae, or other sources may modify the Bondi rate if they are at high enough velocity (Melia 1992a). Bogdan & Gilfanov (2008) suggest that SNR drive a bipolar wind out of the plane of M31 with a speed of ∼60 km s^{-1}. This wind is seen at large distances from M31*, but if it extends to, or originates in, the nuclear region of M31 it still should not greatly effect the Bondi flow because its velocity is a factor of 5 lower than the sound speed of ∼300 km s^{-1}. On the other hand, if the bipolar flow centers on M31* then there may be some connection with outflows or jets originating from the RIAF.

3.2. Accretion Flow

Sgr A* appears to be a slightly resolved (non point) source in the *Chandra* images with a luminosity of $\sim 10^{34}$ erg s^{-1}. This implies that the accretion flow itself is bright in X-rays. In contrast, in M31* there is no discernible difference in the X-ray emission within the Bondi radius. It appears consistent

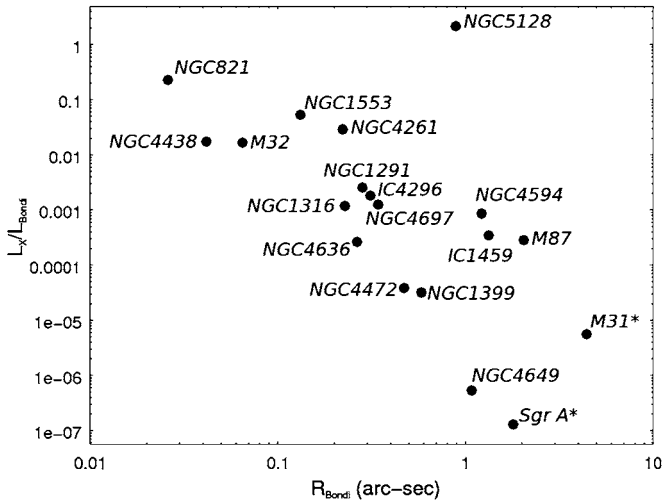

Figure 8. Bondi radii of nearby SMBH vs. their apparent X-ray luminosity (or upper limits) in units of the expected Bondi luminosity. Objects in the lower right of this diagram provide simultaneously secure and severe constraints on accretion and emission models for these SMBH. In this regard, M31* is the outstanding object. Note that this figure is an update of Figure 6 in Garcia et al. (2005).

with that from the diffuse gas in the larger surrounding area. This is an important point that deserves special emphasis: the observations to date detect fundamental differences in the X-ray emission from Sgr A* and M31*; the former is extended and the latter consistent with a point source.

Unfortunately, it is unclear whether we would even detect the extended accretion flow around Sgr A* if it was at the distance of M31*. The fractional Eddington luminosity of an ADAF flow scales with fractional Eddington mass accretion rate (see, for example, Figure 7 of Narayan & McClintock 2008). M31* and Sgr A* are accreting at approximately the same Eddington scaled rate, so the Sgr A* flow would be ∼50× brighter around M31* due to its higher mass, or $\sim 5 \times 10^{35}$ erg s^{-1}. This is on the order of the upper limit to excess diffuse emission due to the Bondi flow that we derived above. However, it is important to note that any prediction based on a Sgr A*-like ADAF is uncertain by at least an order of magnitude because the 0.1–1.0 keV X-ray luminosity of the Sgr A* flow is hidden behind 10^{23} cm^{-2} of absorption.

3.3. A Random Superposition?

While we have detected X-ray emission at a location consistent with M31* which we argue does indeed originate from M31*, we must also ask what the chances are of a random X-ray binary within the nuclear region of M31 being located at the position of P3 = M31*? In order to answer this question, one needs to estimate the density of sources in the nuclear region. As the density increases with decreasing radius one needs to assume some fiducial radius within which to compute the density.

We take the Bondi radius as this fiducial radius. We then count the number of sources within this radius both in M31, and also in our Galaxy under the assumption that the density of bright nuclear sources is similar. Within the Galaxy, the number of $>10^{36}$ erg s^{-1} at the M31* Bondi radius if it was transferred to the Galaxy (i.e., within $100 \times 5''$) is 2 (Muno et al. 2009). Given this number, the probability of a random source being within 0.″2 (the registration/centroiding error) of M31* is 0.3%. If we count sources $>10^{36}$ erg s^{-1} within the Bondi radius at M31 itself, we find 4 (or 5, depending upon the epoch) and a probability of 0.6%. We note that the number counts in the Galaxy might be artificially low due to the high absorption obscuring our view of soft sources, but these two estimates are in reasonable agreement given the low number statistics. We further note that these estimates are conservative, because if we increase the fiducial radius by 3.2× and therefore the surface area by 10×, the average source density and therefore probability decreases by 5×.

While the odds of an interloper are small, we note that there is nothing in the X-ray spectrum or light curve of the source at P3 to distinguish it from an interloping X-ray binary. Our identification of this source as M31* is based solely on positional coincidence. The variations in luminosity that we have found of $(0.6\text{–}20) \times 10^{36}$ erg s^{-1} (0.1–7.0 keV) are consistent with the upper limit of 1.2×10^{36} erg s^{-1} set by Li et al. (2009), particularly considering that M31* was relatively faint in the 2004/2005 observations.

As well as confirming our tentative detection of M31* (Garcia et al. 2005), we have detected variable emission consistent with a location in P1. The emission could be due to a single low mass X-ray binary embedded in P1.

3.4. Variability

In the X-ray, the most rapid variability which is clearly detected is a factor of 3 on a 10 day timescale. This is consistent with the orbital timescale at ∼100 Schwarzchild radii ($r_S = 2GM/c^2$) from M31*. X-ray flares are seen in Sgr A* with durations of hours and amplitudes of a factor of ∼10 (Baganoff et al. 2001; Marrone et al. 2008). Given that we would expect the timescale of such flares to scale with mass, similar flares in M31* would occur on a ∼40 hr or a few day long timescales. Thus, this most rapid variability we see from M31* might plausibly be associated with the flares seen in Sgr A*.

3.5. Spectral Slope

The spectral slope of the emission from M31* appears to be the same in the radio and X-ray frequency ranges, but the X-ray flux is far above the extension of the radio spectrum into the X-ray range. As is the case with Sgr A*, this energy distribution is consistent with a synchrotron source for the radio emission and Compton up-scattering of the radio photons by the relativistic electrons into the X-ray range in synchrotron self-Compton or SSC process (Falcke & Markoff 2000; Liu & Melia 2001; Hornstein et al. 2007). If this is indeed the emission mechanism, any short timescale radio variability should be echoed in the X-ray flux.

4. CONCLUSIONS

We have detected X-ray emission from both optical nuclei of M31 (P1 and P3) and this variable emission is consistent with two point sources. Having resolved M31* from the surrounding point and diffuse X-ray sources we can now investigate the accretion properties of this nearby SMBH. The presence of a hot and truly diffuse emission component in the core of M31 was first noted in *Einstein* observations (Trinchieri & Fabbiano 1991) and later confirmed with *ROSAT* (Primini et al. 1993), *XMM-Newton* (Shirey et al. 2001a), and *Chandra* (Dosaj et al. 2002) observations. Any of this gas within the Bondi radius of the SMBH will accrete and possibly generate accretion luminosity. In order to compute the Bondi accretion rate, we use the X-ray observations to estimate the temperature and density of this gas. The resulting rate accretion rate would produce a luminosity of

4×10^{41} erg s^{-1} if the gas radiated with the canonical $\sim$10% efficiency. Given the observed luminosity of $\sim 2 \times 10^{36}$ erg s^{-1}, M31* is one of the most underluminous SMBHs known.

Because M31* has the most highly resolved Bondi flow of any SMBH, a long X-ray observation could determine the applicability of ADAF, CDAF, ADIOS, or other models to quiescent SMBH accretion. This in turn will tell us the form that black hole accretion takes for the vast majority of cosmic time. For example, a 400 ks ACIS-S observation would yield 2500 counts within the Bondi radius (nearly 10 per pixel), sufficient to divide the region into 5 annuli and determine accurate temperatures in five radial rings. This would be sufficient to determine the run of temperature with radius in the RIAF. The various RIAF models all predict $T(1/r)^{\alpha}$, so these data could determine α and therefore the structure of the RIAF.

If we accept that the A-stars in P3 are from a recent star formation episode then age of the P3 star cluster may be $\sim$200 Myr (Bender et al. 2005), and the mass required to produce this cluster during a single star formation burst may be between a few $10^4\ M_{\odot}$ and $10^6\ M_{\odot}$ (Bender et al. 2005; Chang et al. 2007) respectively. This implies that there was a source providing this mass at a rate of $\sim 10^{-4}$ to $10^{-2}\ M_{\odot}$ yr^{-1}. We note that the Bondi accretion rate is comparable to the lower range of the rate needed to form the star cluster, suggesting that the SMBH itself may influence the rate of star formation in its immediate surroundings (see also Fatuzzo & Melia 2009 concerning this issue with regard to the Galactic center). Of course, suggesting that Bondi accretion is important begs the question of where the gas that is being accreted came from in the first place. We also note the coincidence between the suggested age of the P3 star cluster (200 Myr) and the time of the last crossing of M32 through the nuclear region of M31 (Block et al. 2006), suggesting that this crossing may have provided the trigger for the star formation event which formed the UV bright cluster at P3.

This work was supported in part by *Chandra* grant GO-6088A and *Chandra* X-ray Center Contract NAS8-03060.

Facilities: CXO, *HST*

REFERENCES

Baganoff, F. K., et al. 2001, Nature, 413, 45
Baganoff, F. K., et al. 2003, ApJ, 591, 891
Ball, G. H., Narayan, R., & Quataert, E. 2001, ApJ, 552, 221
Barmby, P., et al. 2006, ApJ, 650, L45
Barmby, P., & Huchra, J. P. 2001, AJ, 122, 2458
Beckerman, E., Aldcroft, T., Gaetz, T. J., Jerius, D. H., Nguyen, D., & Tibbetts, M. 2004, Proc. SPIE, 5165, 445
Bender, R., et al. 2005, ApJ, 631, 280
Blandford, R. D., & Begelman, M. C. 1999, MNRAS, 303, L1
Block, D. L., et al. 2006, Nature, 443, 832
Bogdán, Á., & Gilfanov, M. 2008, MNRAS, 388, 56
Chang, P., Murray-Clay, R., Chiang, E., & Quataert, E. 2007, ApJ, 668, 236
Crane, P. C., Dickel, J. R., & Cowan, J. J. 1993, ApJ, 411, L107
Demarque, P., & Virani, S. 2007, A&A, 461, 651
Di Stefano, R., et al. 2004, ApJ, 610, 247
Dosaj, A., Garcia, M., Forman, W. R., Jones, C., Kong, A., di Stefano, R., Primini, F., & Murray, S. 2002, in ASP Conf. Ser. 262, The High Energy Universe at Sharp Focus: Chandra Science, ed. E. M. Schlegel & S. D. Vrtilek (San Francisco, CA: ASP), 147
Dosaj, A., Garcia, M. G., Forman, W. R., Jones, C., Kong, A., Primini, F. A., Di Stefano, R., & Murray, S. S. 2001, BAAS, 33, 1369
Edmonds, P. D., Gilliland, R. L., Heinke, C. O., & Grindlay, J. E. 2003, ApJ, 596, 1177
Falcke, H., & Markoff, S. 2000, A&A, 362, 113
Fatuzzo, M., & Melia, F. 2009, PASP, 121, 585
Garcia, M. R., Kong, A., Primini, F. A., Barmby, P., Di Stefano, R., McClintock, J. E., & Murray, S. S. 2001, in Two Years of Science with Chandra (Cambridge: CXC), abstract 112, http://cxc.harvard.edu/symposium_2001/NG/112/112.html
Garcia, M. R., Murray, S. S., Primini, F. A., Forman, W. R., McClintock, J. E., & Jones, C. 2000, ApJ, 537, L23
Garcia, M. R., Williams, B. F., Yuan, F., Kong, A. K. H., Primini, F. A., Barmby, P., Kaaret, P., & Murray, S. S. 2005, ApJ, 632, 1042
Ghez, A. M., et al. 2003a, ApJ, 586, L127
Ghez, A. M., et al. 2003b, ApJ, 586, L127
Gordon, K. D., et al. 2006, ApJ, 638, L87
Hawley, J. F., & Balbus, S. A. 2002, ApJ, 573, 738
Henze, M., et al. 2009, A&A, 498, L13
Hornstein, S. D., Matthews, K., Ghez, A. M., Lu, J. R., Morris, M., Becklin, E. E., Rafelski, M., & Baganoff, F. K. 2007, ApJ, 667, 900
Igumenshchev, I. V., Abramowicz, M. A., & Narayan, R. 2000, ApJ, 537, L27
Kaaret, P. 2002, ApJ, 578, 114
Kong, A. K. H., DiStefano, R., Garcia, M. R., & Greiner, J. 2003, ApJ, 585, 298
Kong, A. K. H., Garcia, M. R., Primini, F. A., & Murray, S. S. 2002a, ApJ, 580, L125
Kong, A. K. H., Garcia, M. R., Primini, F. A., Murray, S. S., Di Stefano, R., & McClintock, J. E. 2002b, ApJ, 577, 738
Kormendy, J., & Bender, R. 1999, ApJ, 522, 772
Lauer, T. R., et al. 1993, AJ, 106, 1436
Li, Z., & Wang, Q. D. 2007a, ApJ, 668, L39
Li, Z., & Wang, Q. D. 2007b, ApJ, 668, L39
Li, Z., Wang, Q. D., & Wakker, B. P. 2009, MNRAS, 397, 148
Liu, S., & Melia, F. 2001, ApJ, 561, L77
Marrone, D. P., et al. 2008, ApJ, 682, 373
Martins, F., Gillessen, S., Eisenhauer, F., Genzel, R., Ott, T., & Trippe, S. 2008, ApJ, 672, L119
Massey, P., Olsen, K. A. G., Hodge, P. W., Strong, S. B., Jacoby, G. H., Schlingman, W., & Smith, R. C. 2006, AJ, 131, 2478
Melia, F. 1992a, ApJ, 387, L25
Melia, F. 1992b, ApJ, 398, L95
Muno, M. P., et al. 2009, ApJS, 181, 110
Narayan, R., Igumenshchev, I. V., & Abramowicz, M. A. 2000, ApJ, 539, 798
Narayan, R., & McClintock, J. E. 2008, New Astron. Rev., 51, 733
Narayan, R., & Yi, I. 1994, ApJ, 428, L13
Narayan, R., & Yi, I. 1995, ApJ, 444, 231
Pietsch, W., et al. 2007, A&A, 465, 375
Prestwich, A. H., Irwin, J. A., Kilgard, R. E., Krauss, M. I., Zezas, A., Primini, F., Kaaret, P., & Boroson, B. 2003, ApJ, 595, 719
Primini, F. A., Forman, W., & Jones, C. 1993, ApJ, 410, 615
Quataert, E., & Gruzinov, A. 2000, ApJ, 539, 809
Shirey, R., et al. 2001a, A&A, 365, L195
Shirey, R., et al. 2001b, A&A, 365, L195
Shvartsman, V. F. 1971, Sov. Astron., 15, 377
Sjouwerman, L. O., Kong, A. K. H., Garcia, M. R., Dickel, J. R., Williams, B. F., Johnson, K. E., Primini, F. A., & Goss, W. M. 2005, in Proc. X-Ray and Radio Connections, ed. L. O. Sjouwerman & K. K. Dyer, http://www.aoc.nrao.edu/events/xraydio
Stanek, K. Z., & Garnavich, P. M. 1998, ApJ, 503, L131
Takahashi, H., Okada, Y., Kokubun, M., & Makishima, K. 2004, ApJ, 615, 242
Tremaine, S. 1995, AJ, 110, 628
Trinchieri, G., & Fabbiano, G. 1991, ApJ, 382, 82
Trudolyubov, S., Kotov, O., Priedhorsky, W., Cordova, F., & Mason, K. 2005, ApJ, 634, 314
Williams, B. F., Garcia, M. R., McClintock, J. E., Kong, A. K. H., Primini, F. A., & Murray, S. S. 2005, ApJ, 628, 382
Williams, B. F., Naik, S., Garcia, M. R., & Callanan, P. J. 2006, ApJ, 643, 356